



Slot-die coating of formamidinium-cesium mixed halide perovskites in ambient conditions with FAAC additive

Nischal Khakurel¹, Materials Science, Engineering and Commercialization (MSEC), Texas State University, San Marcos, TX 78666, USA

Drew Amyx, Department of Physics, Texas State University, San Marcos, TX 78666, USA

Maggie Yihong Chen, Materials Science, Engineering and Commercialization (MSEC), Texas State University, San Marcos, TX 78666, USA; Ingram School of Engineering, Texas State University, San Marcos, TX 78666, USA

Yoichi Miyahara¹, and **Wilhelmus J. Geerts**¹, Materials Science, Engineering and Commercialization (MSEC), Texas State University, San Marcos, TX 78666, USA; Department of Physics, Texas State University, San Marcos, TX 78666, USA

Address all correspondence to Wilhelmus J. Geerts at wjgeerts@txstate.edu

(Received 19 September 2023; accepted 16 January 2024; published online: 7 February 2024)

Abstract

Continuous pin-hole free $\text{FA}_{0.78}\text{Cs}_{0.22}\text{Pb}(\text{I}_{0.85}\text{Br}_{0.15})_3$ films are deposited by gas-assisted slot-die printing under ambient conditions using DMF/DMSO based ink containing Formamidinium Acetate additive. Using a binary solvent mixture of DMF and DMSO is effective in eliminating the non-perovskite phase that occurs when DMF alone is used. Print-speed, gas flow rate and chuck temperature are optimized to realize homogeneous films with constant bandgap (1.63 eV) over large substrates ($2'' \times 4''$). The perovskite films prepared using two solvents DMF and DMF: DMSO (9:1) were incorporated in single junction devices. The resulting devices show improved fill factor with improved power conversion efficiency.

Introduction

Since their introduction in 2009, the power conversion efficiency (PCE) of hybrid perovskite solar cells has skyrocketed and reached 26.1% in present day^[1] outperforming other technologies including multi-crystalline silicon, indium gallium selenide (CIGS), and CdTe thin film solar cells. While the initial perovskite, methylammonium lead iodide (MAPbI_3), shows poor thermal stability which poses a considerable difficulty for application, the thermal stability has now been addressed by cation substitution. This enhancement included replacing the MA cations with Formamidinium (FA) cations, which are slightly bigger than MA cations and can withstand temperatures up to 150°C.^[2] Also, FA seems much less volatile than MA, and can thus be more easily retained in the deposited films. However, the photoactive α -FAPbI₃ phase is metastable and easily transforms to the non-photoactive δ -phase particularly when the material is exposed to oxygen and or high humidity. The photoactive α -phase can be stabilized by replacing some (10–20%) of the FA in the lattice with Cesium (Cs).^[3] It is believed that the higher stability of the mixed A-site perovskites originates from the entropy contribution to the Gibbs free energy.^[4] To further increase efficiency, perovskite solar cells are currently being studied to be deposited on top of conventional silicon solar cells. This results in tandem devices where a large bandgap perovskite top cell absorbs the short wavelength,

and a narrower bandgap silicon bottom cell absorbs the longer wavelength. Such tandem devices have a power conversion efficiency (PCE) that surpasses the theoretical Shockley-Queisser limit for a single layer cell.^[5] For two terminal perovskite-Si tandem series cells, the optimum bandgap of the wide bandgap perovskites is on the order of 1.65 eV–1.7 eV which leads to the same current density in both top and bottom cells.^[6,7] The tandem cell however will have a larger open-circuit voltage, V_{oc} , resulting in the higher PCE. The versatility of hybrid perovskites to tune the bandgap by replacing some of the Iodide (I) with Bromine (Br) makes it possible to fine tune the bandgap of the perovskite absorber layer and to obtain a perovskite-silicon tandem cell with a PCE up to 33.9% reported by LONGi on November 3, 2023.^[1,8] Commercialization of these tandem devices now depends on increasing the lifetime of the perovskite cells and finding a scalable deposition method that allows to deposit homogeneous pin-hole free perovskite layers over large areas at high deposition rate. In this paper we focus on the latter.

The ability to deposit perovskite thin films by solvent processing at room temperature opens up an economical pathway to mass fabricate hybrid perovskite solar cells. Although spin processing is used in a lot of perovskite research papers, this deposition method is not scalable. The nucleation and growth process during the spin casting process varies with the radial position (r) as tangential velocity between wet film and atmosphere increases towards the edge slightly affecting the mass transfer coefficient^[9] and thus the nucleation density. This will make it difficult to produce homogeneous perovskite films over large areas with spin casting. So, although high-efficient pixel size devices (active area 6 mm^2) can

Wilhelmus J. Geerts was an editor of this journal during the review and decision stage. For the MRS Communications policy on review and publication of manuscripts authored by editors, please refer to <http://www.mrs.org/editor-manuscripts/>

be manufactured using spin-casting, the PCE strongly decreases with size. Other deposition methods that are more scalable are blade coating,^[10] roll-coating,^[11] spray-coating,^[12] ink-jet printing,^[13] and slot-die coating. Here we further explore slot-die printing of wide bandgap hybrid perovskites that are used in Si-perovskite tandem devices, specifically $\text{FA}_{0.78}\text{Cs}_{0.22}\text{Pb}(\text{I}_{0.85}\text{Br}_{0.15})_3$. These films have a bandgap close to 1.68 eV and are stable for deposition in air. These films are normally spin-casted using a two-step process. An initial spin cast used to deposit the perovskite ink is followed by a second anti-solvent step. The anti-solvent induces a high nucleation rate in the perovskite layer resulting in a smooth pin-hole free layer.^[7,14] Although a two-step slot-die coating has been utilized to deposit perovskite absorber layers,^[15] here we report an alternative technique in which gas quenching is employed to get the right nucleation and growth during the drying process. This method, i.e., slot die printing of the wet perovskite layer followed by gas-quenching with nitrogen gas, results in low waste generation and decouples the wet deposition and drying processes allowing for the realization of smooth pin-hole free perovskite films that have a homogeneous film thickness and density over large areas. As wet film deposition and drying are decoupled, such processes can be more easily controlled than a spin coating process including an antisolvent step. The quality of the wet slot-die coating is determined by the print parameters including slot-die gap height, dispense rate, shims thickness, and coating speed^[11,12,13,16] and can be further optimized by adjusting, priming gap, dispense stop offset, dispense delay, and trailing and leading edge heights and offsets. The quality of the drying process can be optimized by adjusting gas flow rate, air-knife shims thickness, air-knife height, air-knife orientation with respect to the substrate, and chuck/substrate temperature. To simplify the optimization process and to avoid high gas-quenching flow rates that could exert a large force and shear force on the meniscus and wet perovskite layer^[17] and distort the wet film, we added Formamidinium Acetate (FAAc) to the ink. Numerous studies have used volatile salts such as methylammonium acetate (MAAc),^[18,19] butylammonium acetate (BAAc),^[20,21] formamidinium acetate (FAAc)^[22,23] to spin cast perovskite films. Nuclear magnetic resonance and Fourier transform infrared spectroscopy have shown that although these volatile salts assist with nucleation and growth by coordinating ability of the acetate with the perovskite which decelerates the nucleation rate with perovskites, they are not incorporated in the annealed films. We deploy a similar strategy here to induce nucleation and growth via an intermediate phase using FAAc additive to perovskite precursor containing Formamidinium-Cesium mixed halides. We further fine-tuned the DMSO/DMF solvent concentration in the ink to obtain smooth glossy films with a small surface roughness and optimize the perovskite phase to yield devices with improved power conversion efficiency (PCE).

Materials and methods

Materials and procedures

Unless otherwise stated all the materials were purchased from Sigma Aldrich and used as received. The perovskite solution

was made in a nitrogen filled glovebox with an oxygen concentration of below 1 ppm. It was made by dissolving 0.775 M Lead Iodide (PbI_2), 0.22 M Cesium Iodide (CsI), 0.225 M Lead Bromide (PbBr_2), 0.78 M Formamidinium Iodide (FAI) [GreatCell Solar] in 1 mL of anhydrous N,N, Dimethylformamide (DMF). The solution was stirred at 550 rpm, 70°C until it turned transparent yellow after complete dissolution of the solids. The same precursors were also used to make an ink based on a mix of DMF and Dimethylsulfoxide (DMSO) (9:1 ratio). 60 mgml^{-1} of Formamidinium Acetate (FAAc) was added to the inks. Similar to the use of MAAc in MAPbI_3 ,^[19] the FAAc does not alter the composition of the final film and only assists in nucleation and growth. This is supported by the XRD and UV-Vis spectra as no noticeable change in structural and optical properties were observed due to the addition of FAAc. The suspension was stirred for 30 min to dissolve the FAAc. The resulting solution was filtered using a 1 μm PTFE filter, loaded into the ink container of our nTact nRad slot-die coater, and then transferred out of the nitrogen glovebox into an air-filled glovebox that contains the slot-die printer. The coatings were deposited under ambient conditions at 30–40% R.H. Nitrogen gas was used to gas quench the perovskite films resulting in a dry film. The films were immediately annealed on a hot plate located in the same air-filled glovebox. Annealing was done at different temperatures i.e. 100°C, 120°C for 10 min. Perovskite films were deposited on cleaned 1 × 1 inch² glass substrates [PV Tech] for UV/VIS, AFM, stylus profilometry, and on glass/ITO for SEM studies.

Glass substrates were cleaned using ultrasonic sonication with Deconex OP121 cleaning solution (5%) in DI water for 20 min. Then they were sonicated again in DI water for 20 min and dried using CO_2 . The slides were O_2 plasma treated for 10 min before they were transferred to a N_2 -filled glovebox.

For device fabrication, pre-patterned 1 × 1 inch² ITO/glass plates were used as substrate. These were cleaned using the same method as the glass slides mentioned above. PTAA [Solaris] 2 mg/ml was dissolved in Toluene and spin coated at 4500 RPM for 45 s followed by a 10 min anneal at 110°C. The PTAA covered Glass/ITO substrate where then transferred to the air-filled glovebox for slot-die coating. The nTact nRad slot-die coater uses air-bearings that will supply 2 scfm of air into the glovebox atmosphere. In addition, during operation, 8 scfm of dry and clean air is blown into the glovebox through a self-made shower head connected to the glovebox's ceiling. The glovebox contains two KF40 vacuum ports on the lower rear that are connected to the exhaust of a fume hood. The throttle of the fume hood is adjusted so the pressure in the fume hood is close to atmospheric pressure verified through a pressure gauge. Since the humidity in our glovebox decreases with time after switching on the clean and dry air, after switching on the clear and dry air we wait until the RH drops below 40% before the printing is started. So, all samples are printed in a relative humidity between 30 and 40%. The solvent concentration in the glovebox as measured with a PID/LEL (photoionization detector/lower explosive limit) meter slightly increases to 10 ppm

during the printing process but then drops down below the PID/LEL meter's detection limit within 2 min of completing the print process. The perovskite precursor with DMF, DMSO and FAc was slot die coated at a dispense rate of $1.8 \mu\text{L/s}$ with a coating speed of 18 mm/s and a gap height of $90 \mu\text{m}$ using a 22 mm die head. The wet film thickness was estimated to be $4.55 \mu\text{m}$. The wet film thickness was estimated by calculating the ratio of dispense rate to coating width and substrate speed i.e., $\frac{\text{dispenserate}}{(\text{coatingwidth} \times \text{substratespeed})}$. To obtain continuous pin-hole free films, gas quenching was used. In this method a high flux of dry gas is blown on the wet film. The high-speed dry gas induces a large evaporation rate resulting in a high nucleation density and thus a pin-hole free film. The gas knife is directly positioned behind the slot-die head and moves in unison with the print head. Our setup is sketched in Fig. 1(a) above. The distance between the slot-die shims and the gas-knife shims is approximately 2.5 inches. Dry room temperature UHP 300 Nitrogen gas (Airgas) is used for the gas quenching. It is applied via a commercial 9" long Exair stainless steel air knife that is furnished with a 0.002" shim. The flow rate was set to 150 LPM which results in a flux of $109 \text{ cm}^2/\text{sec}$ and a max gas speed at the knife slit of 215 m/s . The distance between the air-knife and the substrates was $320 \mu\text{m}$ for the DMF-based ink and $1390 \mu\text{m}$ for the DMF: DMSO 9:1 ink. As shown by the calculation of Park, the air velocity will decrease with gas-knife to substrate thickness and will be lower away from the direct proximity of the gas-knife slit.^[14] Using the data of Fig. 13 of reference^[17] we estimate that the speed of the gas near the surface for the latter gas-knife to substrate distance to be on the order of 150 m/s . Once the gas reaches the substrate it bends and travels parallel to the substrate quickly reducing its maximum speed. At 1 mm away from the slit along the surface we expect the gas speed to have lowered below 100 m/s . For gas flows more than 180 LPM our vacuum pump is no longer able to keep the substrates on the vacuum chuck and the substrates were lifted at higher pressures as described by Bernoulli's law.

The slot-die setup consists of an aluminum chuck whose temperature was varied from room temperature 30 to 70°C for perovskite precursor without DMSO. The chuck temperature was fixed at 40°C for perovskite precursor with DMF: DMSO 9:1 + FAc. The annealing temperature was optimized at 120°C for 10 min for both types of films. The printing and annealing conditions for devices were chosen after the verification from XRD spectra. The annealed perovskite layers were transferred to a Trovato 300C thermal evaporation chamber from Trovato that is in the nitrogen glovebox to deposit 40 nm C_{60} [Solaris], 8 nm BCP and 100 nm Aluminum [Kurt. J. Lesker] using a shadow mask. Each $1 \times 1 \text{ inch}^2$ substrate contains four devices that each have an active area of 6.25 mm^2 due to the overlap of ITO and Aluminum electrodes. The device architecture is shown in Fig. 1(a). Before these devices were taken out of the glovebox, they were encapsulated using a self-built encapsulation robot.

Characterization

The UV-Vis spectra of the thin perovskite films directly deposited on glass substrates were measured using a Shimadzu UV-2501 spectrometer. The absorption spectra from 900 nm to 450 nm were recorded for all the films with a resolution of 0.1 nm . The beam was 12 mm tall and 1 mm wide. UV-Vis spectra was measured at three different points on the sample. The crystalline structure of the same thin films was probed using a Rigaku SmartLab X-Ray Diffractometer (XRD) with a Cu target at 40 keV . θ - 2θ scans were taken from 5° to 55° with a step size of 0.02° . An FEI Helios NanoLab 400 SEM was used to take images of the perovskite films printed on glass/ITO substrates. The accelerating voltage used was 5.00 kV and the beam current was 43 pA . Complete solar cell devices were characterized by illuminating with an Oriel ABA solar simulator. The current-voltage (I - V) characteristics were obtained using a Keithley 2400 source meter controlled by a computer running a

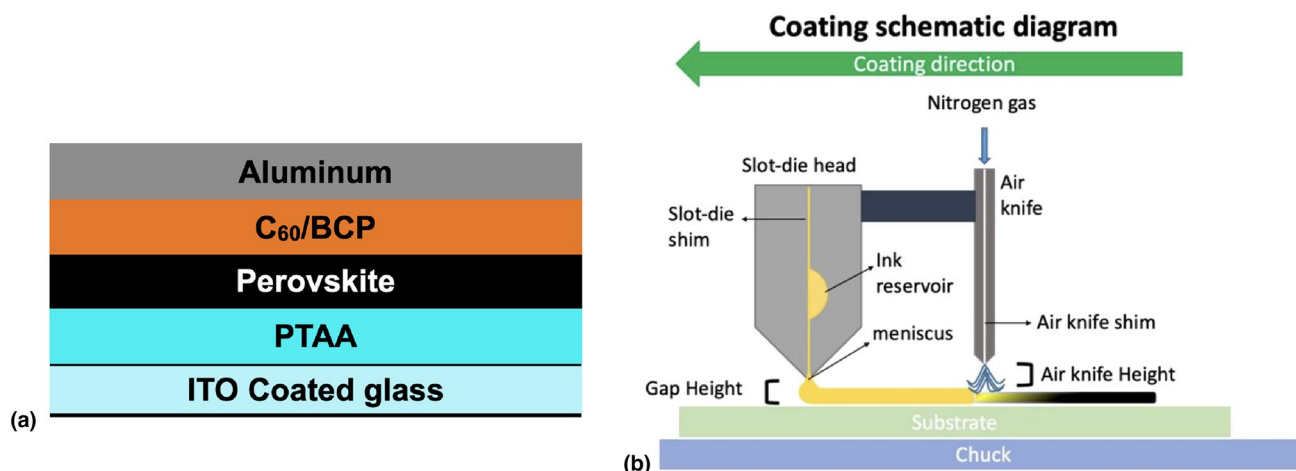


Figure 1. (a) configuration of perovskite solar cell (p - i - n) (b) Schematic diagram of slot-die coating.

LabView program. Forward and reverse current–voltage (J – V) curves were measured under AM 1.5G.

Results and discussion

Films printed with the DMF based ink on glass substrates were studied by SEM. The images as shown in Fig. 2 reveal that the films that were coated using nitrogen gas assisted quenching were continuous and devoid of pinholes that are detrimental to device performance. We also observed that the film coated without nitrogen quenching had pinholes. Moreover, the films did not show pinholes regardless of the coating temperature. The crystal size increases slightly with chuck temperature and seems to have a maximum size at a chuck temperature of 50°C. In addition to the SEM images,

the photographs of the slot-die coated thin films are shown in Figure S5. Figure 2(a) shows the UV–Vis spectra of thin films with an inset of Tauc plot at different chuck temperatures. The absorption onset is around 760 nm, which when replotted in the form of a Tauc plot, shows a bandgap ranging from 1.62 to 1.64 eV. This is in close agreement to literature that uses similar perovskite composition.^[14] The roughness of the films was measured with AFM and increases with chuck temperature from $R_a = 14.32$ nm for films printed at 30°C to $R_a = 38.74$ nm for films printed at 70°C. Results are summarized in Figure S4. Figure 3 below shows the θ – 2θ scan of perovskite films slot-die printed on glass substrates. The diffraction patterns for films printed at different chuck temperatures using the DMF based ink are shown in Fig. 3(a). It was confirmed via XRD that the slot-die coated thin films

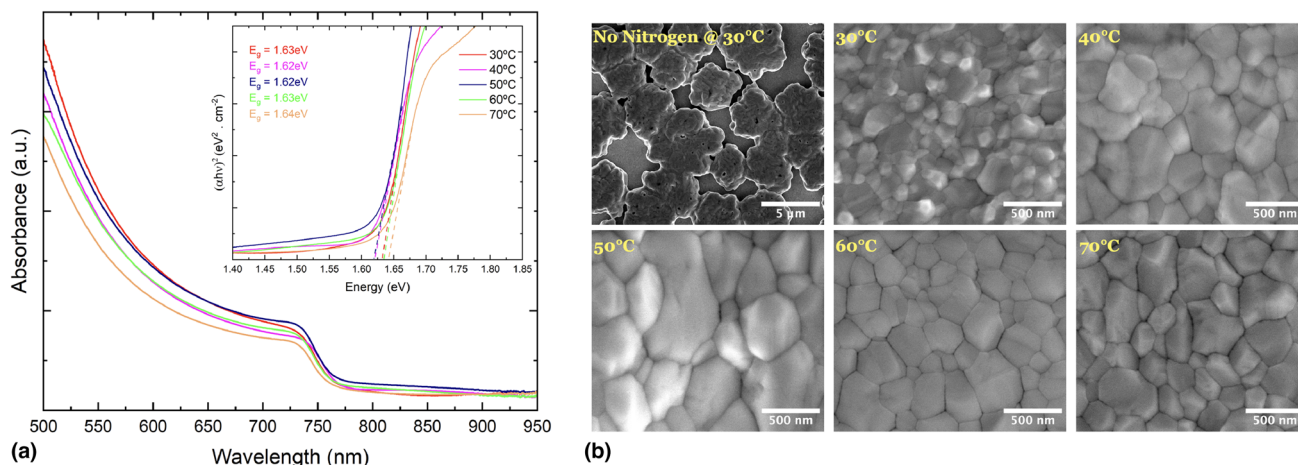


Figure 2. (a) UV–Vis spectra of DMF based perovskite thin films with an inset of Tauc plot and (b) SEM images of corresponding films, as a function of chuck-temperature.

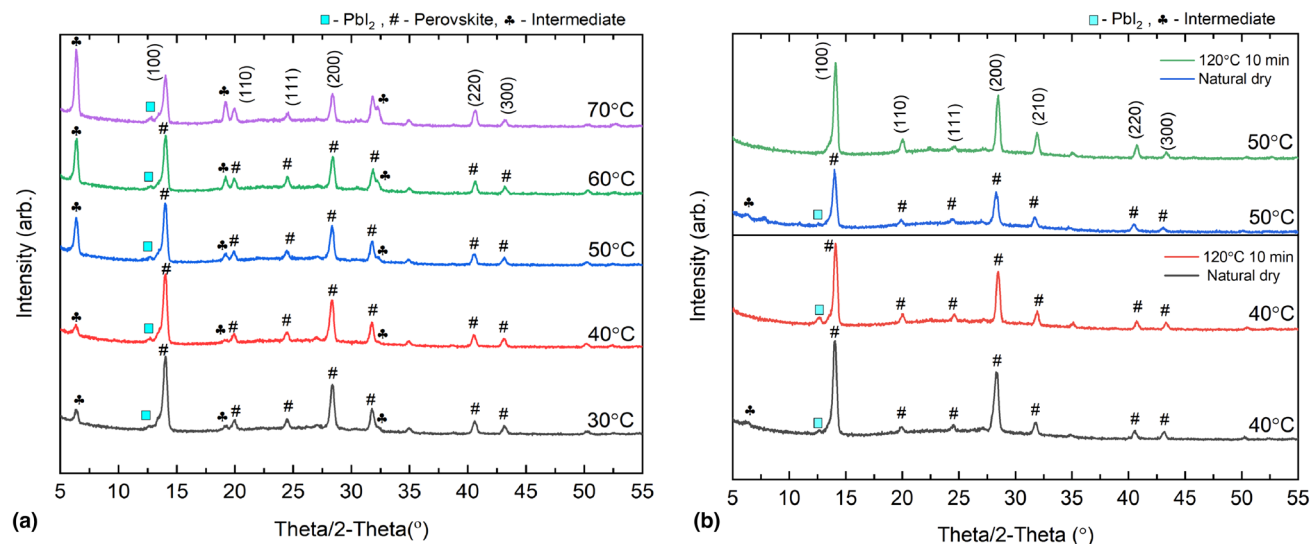


Figure 3. (a) XRD analysis of perovskite with FAAC in DMF coated at different chuck temperatures (b) XRD analysis of perovskite with FAAC in 9:1 DMF: DMSO at different chuck temperatures, (films without anneal and after annealing at 120°C for 10 min, indicated by labels).

retained its cubic structure at different chuck temperatures. The diffraction peaks observed at $\sim 14.04^\circ$, 19.94° , 24.40° , 28.33° , 31.70° , 40.51° , 43.0° are assigned to the (100), (110), (111), (200), (210), (220) and (300) of the cubic (α -phase) perovskite phase. However, other unidentified peaks were observed at 6.38° , 19.2° , and 32.5° (indicated by club symbols). These unidentified peaks are small for samples prepared at room temperature (30°C) while the peaks become more pronounced for the samples printed at 70°C , implying that the phase purity of the perovskite films decreases with increasing chuck temperature. These peaks at lower angle do not correspond to PbI_2 , whose characteristic peak is at 12.6° (denoted by square symbol). For now, we refer to these peaks as intermediate to identify that they originate from an intermediate phase. Note that peaks of an intermediate phase have also been reported in literature for PbI_2 -DMF complex, hydrate compound,^[25] a polymorph of $\text{FAI-PbI}_2\text{-CsI-PbBr}_2\text{-DMF}$ ^[26] and may relate to the presence of the DMF molecules.^[27] The intermediate peaks here observed could not be assigned to any crystal plane of perovskite or PbI_2 hence, we hypothesize that they are due to an intermediate phase of perovskite with FAAC and or the solvents.

It has been reported^[28] that for MAPbI_3 addition of DMSO to DMF ink enables homogeneous crystallization of perovskite thin films through the higher coordination ability of DMSO with lead iodide. A transparent film is formed upon deposition believed to be an adduct of PbI_2 with Lewis base DMSO and iodide in MAI. This intermediate phase is then converted in the photoactive phase by drying through and anti-solvent step. The formation of this intermediate phase retards the crystallization and gives better control over homogeneous film formation. The solubility of Lead Iodide in DMSO:DMF is higher compared to other single solvents such as 2-ME (2-Methoxyethanol). Moreover, other binary solvents have been proven to significantly improve perovskite morphology but require extensive optimization.^[29] The relationship between different solvent systems and homogeneous nucleation and growth is complex which opens various avenues for future study. Here we employ a similar strategy by replacing some part of DMF with DMSO (9:1 DMF:DMSO) in our ink with FAAC additive. Unless explicitly stated, we use the same fabrication process/parameters for slot-die coating.

The intermediate peak at 6.38° is also observed in the XRD patterns of unannealed films slot-die printed from the 9:1 DMF:DMSO ink. These films are referred to as natural dry in Fig. 3 (b). We can see that the intensity of these intermediate peaks (denoted by club '♣' sign) are much lower than in DMF based ink. This means the phase purity of our films increased upon the addition of DMSO to the ink. Moreover, to also corroborate our results further, we conducted XRD analysis on the films coated at 40 and 50°C . We started with 40 and 50°C chuck temperatures due to the sharp increase in intermediate composition in DMF based perovskite indicated by XRD spectra. Furthermore, we noticed that regardless of the chuck temperature, the intensity of intermediate phase does not significantly

depend on the print temperature and can be avoided after a 120°C anneal. Hence, we used the same annealing and depositing condition while fabricating single junction devices i.e. 40°C chuck temperature. Note that we increased the annealing temperature to 120°C while keeping the same annealing time (10 min) to improve the (100) texture.

To further extend the validation of these phase and texture optimized thin films, we evaluated the device performance of slot-die coated thin films with FAAC additive for DMF based ink and for ink that includes the blend of DMF: DMSO (9:1). We incorporated the films into devices with an active area of 0.0625 cm^2 at 12 locations on three $1 \times 1\text{ inch}^2$ substrates for each solvent/process conditions. We implemented them into an (*p-i-n*) device architecture with ITO/PTAA/Perovskite/ C_{60} /BCP/Al device structure. The box plot of device parameters is shown in Figure S1 with data tabulated in Table S1. The champion device with DMF solvent (at 60°C chuck temperature) showed a forward bias PCE of 10.93% with an open circuit voltage (V_{OC}) of 1.03 V and short circuit current density (J_{SC}) of -19.88 mAcm^{-2} . The limiting factor behind the PCE was a low fill factor (FF) of 53.30%. We observed a low FF while coating at different chuck temperatures. The variation of power conversion efficiency for the devices with the films deposited at different chuck temperature is shown in Fig. 4(a) below.

The device performance showed significant improvement after the addition of DMSO to the ink. Figure 4(b) shows the power conversion efficiency of the solar cells made with partial replacement of DMF by DMSO in the ink. The higher performance is due to the increased FF. The champion device showed a power conversion efficiency of 12.11%, a J_{SC} of 18.8 mAcm^{-2} and FF of 62.8% with a V_{OC} of 1.01 V (Figure S2). The devices fabricated using both solvents showed hysteresis behavior between the forward and reverse scan measurements. The champion device made using 9:1 DMF: DMSO showed a hysteresis index (HI) of 4.95×10^{-3} . This behavior has been associated with interface of perovskite with the transport layers.^[30] Hence, interfacial engineering to passivate such defects has been given importance to reduce hysteresis behavior in perovskite/HTL interface. The R_a values measured by AFM of slot-coated perovskites using the DMF: DMSO 9:1 blend was 22.55 and 19.91 nm for 50 and 40°C chuck temperature respectively. This roughness is comparable to the low temperature slot-die coated films from based DMF-based ink. The bandgap of the perovskite film was not affected by the DMSO in the ink and remained constant, 1.63 eV as shown in Figure S3. DMSO has also been known to cause voids at perovskite/HTL interface, however, our results did not indicate the presence of voids.^[24] However, prolonged aging experiments are needed to corroborate the phase instability with voids or void formation during processing.

To develop a large area module for perovskite solar cells, the films should have specular reflection with minimal variation in properties to have a consistent PCE while incorporating those films in devices. In our work, we successfully demonstrated the role of FAAC additive in the perovskite

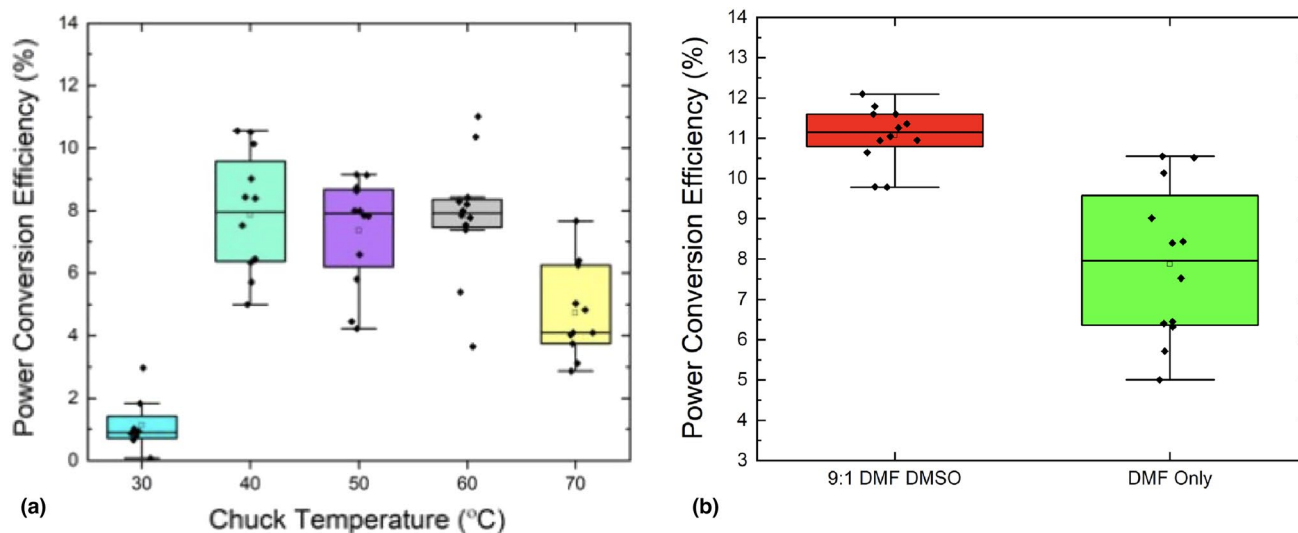


Figure 4. (a) Variation of PCE of slot-die coated perovskite with DMF and FAc additive, (b) Improvement of PCE after addition of DMSO.

solution. This method ensured the fabrication of consistent polycrystalline perovskite thin films without any morphological defects like pinholes, specifically when utilizing slot-die coating. Furthermore, we uncovered the influence of DMSO in refining the texture of slot-die coated thin films. To further our work, we are currently investigating the impact of varying the ratio of DMF: DMSO and their consequence on process parameters (typically speed). We are aiming to pursue this to achieve rapid coating speeds, a crucial factor for large area module fabrication.

Conclusion

In conclusion, we have developed a novel solvent engineering based additive approach strategy for slot-die coating to optimize the phase of wide bandgap perovskites by introducing volatile organic salt and suitable coordinating solvent into the perovskite precursor. Our results show that the addition of FAc salt in a DMF-based ink leads to the formation of a non-perovskite phase that has diffraction peaks at 6.38° , 19.2° , and 32.5° in films that are slot-die printed in ambient air. Films with large phase impurities have a large roughness and when used in devices will result in low power conversion efficiencies. The non perovskite phase can be avoided by adding DMSO to the ink and optimizing the annealing temperature. Using this strategy, we were able to increase the power conversion efficiency of slot-die printed wide bandgap solar pixel devices to $\sim 12\%$ through mainly an increased FF.

Acknowledgments

This paper is dedicated in the memory of Dr. Alex Zakhidov who was a great mentor and professor. The authors would like to acknowledge the editor's invitation to contribute to the

special issue of MRS Communications under the title "Organic and Perovskite Materials and Devices". N.K. acknowledges funding from Doctoral Research Support Fellowship and The Graduate College Scholarship, Texas State University.

Author contributions

All authors contributed to the study conception and design. NK and DA: Material preparation, data collection and analysis were performed. NK: The first draft of the manuscript was written and all authors commented on previous version of manuscript. All authors read and approved the final version of the manuscript.

Funding

This work was supported by National Science Foundation (NSF) through STTR Phase II grant #1927020, NSF EPMD grant #1906492, U.S. Department of Navy, HBCU/MI Program (ONR grant# N000141912576) and in part by The U.S. Department of Energy's office of Energy Efficiency and Renewable Energy (EERE) under the Solar Technologies Office Award number DE-EE0009526. The views expressed herein do not necessarily represent the views of the U.S. Department of Energy or the United States Government.

Data availability

The data that supports the findings of this study are available on request from the corresponding authors.

Declarations

Conflict of interest

All authors declare no conflicts of interest.

Supplementary Information

The online version contains supplementary material available at <https://doi.org/10.1557/s43579-024-00522-x>.

References

1. "National Renewable Energy Laboratory (NREL), Best Research-Cell Efficiency Chart, <https://www.nrel.gov/pv/cell-efficiency.html>."
2. G.E. Eperon, S.D. Stranks, C. Menelaou, M.B. Johnston, L.M. Herz, H.J. Snaith, Formamidinium lead trihalide: a broadly tunable perovskite for efficient planar heterojunction solar cells. *Energy Environ. Sci.* **7**(3), 982–988 (2014). <https://doi.org/10.1039/C3EE43822H>
3. Z. Li, M. Yang, J.-S. Park, S.-H. Wei, J.J. Berry, K. Zhu, Stabilizing perovskite structures by tuning tolerance factor: formation of formamidinium and cesium lead iodide solid-state alloys. *Chem. Mater.* **28**(1), 284–292 (2016). <https://doi.org/10.1021/acs.chemmater.5b04107>
4. C. Yi et al., Entropic stabilization of mixed A-cation ABX₃ metal halide perovskites for high performance perovskite solar cells. *Energy Environ. Sci.* **9**(2), 656–662 (2016). <https://doi.org/10.1039/C5EE03255E>
5. W. Shockley, H.J. Queisser, Detailed balance limit of efficiency of p-n junction solar cells. *J. Appl. Phys.* **32**(3), 510–519 (1961). <https://doi.org/10.1063/1.1736034>
6. Y. Cheng, L. Ding, Perovskite/Si tandem solar cells: Fundamentals, advances, challenges, and novel applications. *SusMat* **1**(3), 324–344 (2021). <https://doi.org/10.1002/sus.2.25>
7. K.A. Bush et al., 23.6%-Efficient monolithic perovskite/silicon tandem solar cells with improved stability. *Nat. Energy* **2**(4), 1–7 (2017). <https://doi.org/10.1038/nenergy.2017.9>
8. W. Rehman et al., Photovoltaic mixed-cation lead mixed-halide perovskites: Links between crystallinity, photo-stability and electronic properties. *Energy Environ. Sci.* **10**(1), 361–369 (2017). <https://doi.org/10.1039/c6ee03014a>
9. J. Danglad-Flores, S. Eickelmann, H. Riegler, Evaporation behavior of a thinning liquid film in a spin coating setup: comparison between calculation and experiment. *Eng. Rep* **3**(9), 1–12 (2021). <https://doi.org/10.1002/eng.2.12390>
10. S. Chen et al., Crystallization in one-step solution deposition of perovskite films: upward or downward? *Sci. Adv.* **7**(4), 26–29 (2021). <https://doi.org/10.1126/sciadv.abb2412>
11. Y. Galagan et al., Roll-to-Roll Slot die coated perovskite for efficient flexible solar cells. *Adv. Energy Mater.* **8**(32), 1801935 (2018). <https://doi.org/10.1002/aenm.201801935>
12. S. Das et al., High-performance flexible perovskite solar cells by using a combination of ultrasonic spray-coating and low thermal budget photonic curing. *ACS Photonics* **2**(6), 680–686 (2015). <https://doi.org/10.1021/acsphotonics.5b00119>
13. F. Schackmar et al., Perovskite solar cells with all-inkjet-printed absorber and charge transport layers. *Adv. Mater. Technol.* **6**(2), 2000271 (2021). <https://doi.org/10.1002/admt.202000271>
14. J. Xu et al., 2020 Triple-halide wide-band gap perovskites with suppressed phase segregation for efficient tandems". *Science* **367**(6482), 1097–1104 (2020). <https://doi.org/10.1126/science.aaz5074>
15. I. Zimmermann et al., Sequentially Slot-die-coated perovskite for efficient and scalable solar cells. *Adv. Mater. Interfaces* **8**(18), 1–9 (2021). <https://doi.org/10.1002/admi.202100743>
16. X. Ding, J. Liu, T.A.L. Harris, A Review of the operating limits in slot die coating processes. *AIChE J.* **62**(7), 2508–2524 (2016). <https://doi.org/10.1002/aic.15268>
17. S. Park, K. Park, Air-knife design for improved drying efficiency in manufacturing flat-panel displays. *J. Comput. Des. Eng.* **9**(4), 1388–1396 (2022). <https://doi.org/10.1093/jcde/qwac058>
18. Y. Xiao, L. Yang, G. Han, Y. Li, M. Li, H. Li, Effects of methylammonium acetate on the perovskite film quality for the perovskite solar cell. *Org. Electron.* **65**, 201–206 (2018). <https://doi.org/10.1016/j.orgel.2018.11.020>
19. S. Venkatesan et al., Tailoring nucleation and grain growth by changing the precursor phase ratio for efficient organic lead halide perovskite optoelectronic devices. *J. Mater. Chem. C* **5**(39), 10114–10121 (2017). <https://doi.org/10.1039/c7tc02928d>
20. Y. Li et al., Efficient, stable formamidinium-cesium perovskite solar cells and minimodules enabled by crystallization regulation. *Joule* **6**(3), 676–689 (2022). <https://doi.org/10.1016/j.joule.2022.02.003>
21. J. Zhang et al., Intermediate phase enhances inorganic perovskite and metal oxide interface for efficient photovoltaics. *Joule* **4**(1), 222–234 (2020). <https://doi.org/10.1016/j.joule.2019.11.007>
22. L. Duan, H. Zhang, M. Liu, M. Grätzel, J. Luo, Phase-pure γ -CsPbI₃ for efficient inorganic perovskite solar cells. *ACS Energy Lett.* **7**(9), 2911–2918 (2022). <https://doi.org/10.1021/acsenergylett.2c01219>
23. R. Xu et al., Formamide acetate induces regulation of crystallization and stabilization in Sn-based perovskite solar cells. *ACS Appl. Mater. Interfaces* **13**(28), 33218–33225 (2021). <https://doi.org/10.1021/acsami.1c05097>
24. M. Wang, C. Fei, M.A. Uddin, J. Huang, Influence of voids on the thermal and light stability of perovskite solar cells. *Sci. Adv.* **8**(35), eabo5977 (2022). <https://doi.org/10.1126/sciadv.abo5977>
25. B.R. Vincent, K.N. Robertson, T.S. Cameron, O. Knop, Alkylammonium lead halides. Part 1. Isolated PbI₆⁴⁻ ions in (CH₃NH₃)₄PbI₆·2H₂O. *Can. J. Chem.* **65**(5), 1042–1046 (1987). <https://doi.org/10.1139/v87-176>
26. J. Cao et al., Identifying the molecular structures of intermediates for optimizing the fabrication of high-quality perovskite films. *J. Am. Chem. Soc.* **138**(31), 9919–9926 (2016). <https://doi.org/10.1021/jacs.6b04924>
27. D. Shen et al., Understanding the solvent-assisted crystallization mechanism inherent in efficient organic-inorganic halide perovskite solar cells. *J. Mater. Chem. A* **2**(48), 20454–20461 (2014). <https://doi.org/10.1039/c4ta05635c>
28. N. Ahn, D.Y. Son, I.H. Jang, S.M. Kang, M. Choi, N.G. Park, Highly reproducible perovskite solar cells with average efficiency of 18.3% and best efficiency of 19.7% fabricated via lewis base adduct of lead(II) iodide. *J. Am. Chem. Soc.* **137**(27), 8696–8699 (2015). <https://doi.org/10.1021/jacs.5b04930>
29. Y. Deng, C.H. Van Brackle, X. Dai, J. Zhao, B. Chen, J. Huang, Tailoring solvent coordination for high-speed, room-temperature blading of perovskite photovoltaic films. *Sci. Adv.* **5**(12), 7537 (2022). <https://doi.org/10.1126/sciadv.aax7537>
30. C.H. Swartz, N. Khakurel, S.R. Najar, M.I. Hossain, A. Zakhidov, Temperature and bias dependent degradation and regeneration of perovskite solar cells with organic and inorganic hole transport layers. *Phys. Status Solidi* (2021). <https://doi.org/10.1002/pssa.202000721>

Publisher's Note Springer Nature remains neutral with regard to jurisdictional claims in published maps and institutional affiliations.

Springer Nature or its licensor (e.g. a society or other partner) holds exclusive rights to this article under a publishing agreement with the author(s) or other rightsholder(s); author self-archiving of the accepted manuscript version of this article is solely governed by the terms of such publishing agreement and applicable law.